ACS OMEGA

Open Access

http://pubs.acs.org/journal/acsodf

Article

Feasibility Study of a Non-Contact Differentiation of Cannabidiol Concentrations Using Interdigital Electrodes

Kanitsorn Boonrat, Pinyada Jaroenkunpanit, Phairote Wounchoum, Vasan Jantarachote, Pakamas Chetpattananondh, and Kanadit Chetpattananondh*

Cite This: *ACS Omega* 2024, 9, 51515−51524

Read Online

ACCESS | Metrics & More | Article Recommendations

ABSTRACT: This feasibility study presents a novel noncontact method for differentiating standard cannabidiol (CBD) concentrations using optimized interdigital electrodes. The electrode design, with a 100 mm^2 sensing area on a 64 mm × 77 mm FR-4 substrate, was improved through finite element analysis. Methanol-CBD solutions (25−1000 ppm) in 2 mL glass vials were analyzed using a vector network analyzer connected via a high-frequency SMA connector, focusing on scattering parameter (S-parameter) changes. The method demonstrated high effectiveness in CBD concentration differentiation, achieving a concentration resolution of 145 MHz/50 ppm based on resonant frequency shift, with an error of 0.17% of the reading, and 0.5 dB/50 ppm using S_{11} amplitude measurement. The proposed method offers a promising, linear, and precise technique for noncontact CBD standard analysis, with potential applications in future research. In addition, impedance measurements can be applied to enhance concentration differentiation further.

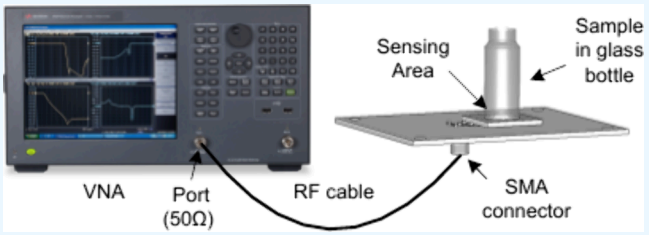

1. INTRODUCTION

Cannabis (Cannabis sativa L.) has a long history of medicinal use, dating back to ancient times. The key compounds found in cannabis include psychoactive substances such as tetrahydrocannabinol (THC) and nonpsychoactive substances like cannabidiol (CBD) and cannabinol (CBN).[1,2] THC possesses properties that alleviate pain, reduce chemotherapy-induced nausea and vomiting, and treat muscle spasticity. Meanwhile, CBD has demonstrated efficacy in relieving seizures, managing pain, reducing symptoms of Parkinson's disease, and combating inflammation. CBN exhibits properties that inhibit lung cancer cell growth.[3] CBD concentration measurement is essential for ensuring the accuracy and consistency of CBD products, particularly for medicinal or therapeutic applications.

Traditional analytical techniques for CBD quantification, such as high-performance liquid chromatography (HPLC), gas chromatography (GC), mass spectrometry, and spectroscopy,[4−6] are commonly used but require advanced laboratory equipment. A liquid chromatography-high resolution mass spectrometry (LC-HRMS) method has been developed to detect adulterants in CBD oils, with detection limits ranging from 0.01 to 0.1 μg/mL, but it still requires sophisticated equipment. Surface-enhanced Raman spectroscopy (SERS)[8] has achieved a detection limit of 10 nM in aqueous solutions, while attenuated total reflectance Fourier-transform infrared spectroscopy (ATR-FTIR) combined with chemometrics has successfully detected synthetic cannabinoids in CBD oils with 100% classification accuracy.[9] A SERS-based capillary device has detected THC at 1 nM,[10] and a gold nanorod array has been used for SERS-based CBN analysis.[11,12] However, these methods are time-consuming, labor-intensive, and require skilled personnel and complex sample preparation.

Various innovative approaches to CBD concentration measurement have been developed in recent years. Many studies highlight the need for biosensor platforms that enable rapid screening and identification of cannabinoids, allowing efficient differentiation of both fiber-type (hemp) and drug-type cannabis.

Reported cannabinoid tests include e.g., colorimetric and fluorescence-based lateral flow assays,[13] electrochemical affinity-based biosensors,[14] competitive volumetric-bar-chart chip assays,[15] and giant magneto resistive-based biosensors.[16] The developed sensors are often based on immunosensing, where target molecules in a sample are detected using specific antibodies. For accurate and sensitive assays, proper immobilization of antibodies or sensing elements on assay supports is crucial, as poor attachment can result in bioactivity loss or detachment in sample fluids.

Received: October 2, 2024
Revised: December 7, 2024
Accepted: December 11, 2024
Published: December 17, 2024

Δ^9-THC and CBD are separated using screen-printed electrodes with chromatographic paper[17] submerged in a closed system with a mobile phase at varying retention durations. Since the measurement is based on chromatographic paper, it cannot be connected to electronic devices for data storage and subsequent analysis or practical planning. A gas sensor,[18] a piezoelectric peptide-hpDNA-based gas sensor,[19] and a nanofiber-based MOS gas sensor[20] were developed to detect THC. The gas sensors frequently suffer nonspecific interactions with other volatile organic compounds present in environmental or biological samples. This can result in false positives or inaccurate readings.

The main challenges in developing portable biosensors are nonspecific interactions and chemical interference from the sample matrix. Furthermore, most of the currently used electrodes are disposable and contact-based, leading to increased testing costs and material waste. The development of alternative techniques that can provide rapid, precise, and nondestructive measurements of CBD concentration is crucial for safety, regulatory compliance, and chemical interference, nondisposable and material waste. Interdigital sensors present a promising alternative due to their simplicity, high sensitivity, and ease of integration into various analytical systems. Interdigital sensors have been extensively studied due to their exceptional sensitivity and precision for evaluating various material and chemical properties.[21] Their simplicity, compactness, low power consumption, cost-effectiveness, and versatility make them suitable for diverse applications, including industrial use, environmental monitoring, food inspection, and medical diagnostics.[22] Current research focuses on five areas: Physical Change Detection: Interdigital sensors are highly accurate for measuring water levels,[23] and moisture in materials like soil[24] and rubberwood,[25] offering nondestructive, portable, and cost-effective solutions for industrial use. Environmental Detection: They have been used in CO_2 and humidity measurement,[26] with advancements in flexible sensors for pH and humidity detection,[27] showing high sensitivity and fast response times. Material Change Detection: New designs monitor material changes, like cable aging[28] and battery coolant detection,[29] combining conductivity and temperature measurements in a single sensor. Medical Applications: Sensors have been used to measure biomarkers for bone loss,[30] humidity for breath monitoring,[31] and glucose[32] for continuous monitoring in diabetic patients. Chemical and Biological Sensing: Applications include detecting natural toxins in seafood,[33] ammonia levels,[34] and volatile organic compounds (VOCs).[35] Innovations include sensors for nitrate[36] and chlorine detection in water[37] and flexible sensors for respiration and skin monitoring.[38]

Cannabidiol (CBD) is a nonpolar molecule due to its structure, which is primarily composed of carbon−hydrogen and carbon−carbon bonds. Furthermore, CBD is insoluble in water but dissolves well in organic solvents such as oils, which is a typical characteristic of nonpolar substances. Although CBD is nonpolar, it can dissolve in methanol, a polar solvent. This occurs because methanol is partially polar and can dissolve substances with both polar and nonpolar components to some extent. Methanol's ability to form hydrogen bonds allows it to dissolve many organic compounds. Methanol is commonly used to prepare standard solutions for HPLC analysis of CBD. This is following AOAC Official Method of Analysis 2018.11, which is applied to cannabinoids in cannabis. Methanol is suitable for use in HPLC systems due to its compatibility with the mobile phase and the columns used in this technique. For accurate CBD concentration detection, creating a reliable calibration curve is essential. Because cannabis has a complex chemical structure, this process usually involves dissolving CBD in methanol to produce a series of known concentrations. The mixture of CBD and methanol in various ratios generates a calibration curve by plotting electrode parameters against concentration. This calibration curve serves as a reference, ensuring the detector can accurately quantify CBD concentration.

In this study, we present our initial findings on the feasibility of distinguishing CBD concentrations in methanol solutions. We used an interdigital electrode-based S11 parameter and impedance measurement to differentiate concentrations ranging from 25 to 1000 ppm. Our designed electrode has a resolution of 145 MHz, which can detect a fine change of 50 ppm in CBD concentration. This technique, which uses an interdigital electrode, is nondestructive and does not produce material waste. It offers good linearity, sensitivity, and cost-effectiveness, supporting the development of a portable sensor with rapid and accurate cannabis analysis capabilities. Additionally, it is easy to interface with data recording devices, such as computers, mobile phones, or other wireless communication systems.

2. EXPERIMENTAL SECTION

A. Theory Consideration. The interdigital capacitive sensor is a planar structure with interleaved comb electrodes, functioning similarly to parallel-plate capacitors. When different potentials are applied to adjacent electrodes, an electric field forms and propagates through the material under test (MUT) on the sensor surface. The sensor's response depends on the electrode design and the dielectric properties of the MUT, which affect capacitance and conductivity. The fringing capacitance varies with the MUT's dielectric constant, making these sensors useful in chemical sensing, food quality monitoring, moisture detection, biosensing, and solution concentration assessment. Figure 1 illustrates the schematic diagram of the sensor's mechanism.

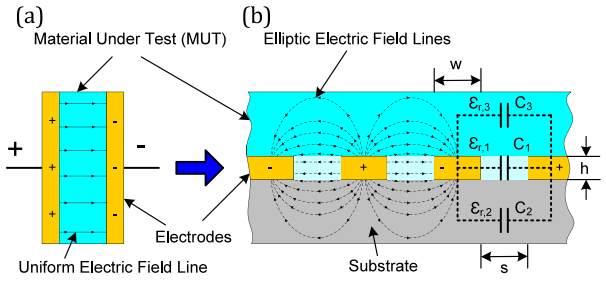

Figure 1. Schematic diagram of the sensor's operating principle. (a) Electric field lines of the parallel plate capacitor and (b) electric field lines of the coplanar interdigital sensor and capacitance between electrodes.

An electric field is generated between the interdigital electrodes when a voltage is applied to the alternating electrode arrangement, as illustrated in Figure 1(b). When a voltage is applied to the alternating interdigital electrodes, an electric field is created, with maximum intensity at the electrode edges and diminishing with distance due to fringing fields. The depth of the field's penetration depends on signal frequency, field strength, the material's permittivity and

https://doi.org/10.1021/acsomega.4c08811
ACS Omega 2024, 9, 51515−51524

conductivity, and the sensor's geometric parameters, including the electrode gap and width.

The structure of interdigital electrodes can be modeled as multiple capacitances connected in parallel, which increases the total capacitance. The capacitance of interdigital electrodes can be calculated using the plane-to-parallel plate transformation method, known as conformal mapping, with the Schwarz-Christoffel Transformation[39] equation. The total capacitance can be calculated using (1), (2), and (3).[40]

$$C_T = (N-1)lC_{pu} \tag{1}$$

Where N is the number of electrodes, l is the electrode length, and C_{pu} is the capacitance for one unit electrode, as shown in Figure 1(b).

$$C_{pu} = (C_3 + C_2 + C_1) \tag{2}$$

$$C_{pu} = \frac{\varepsilon_0(\varepsilon_{r,3} + \varepsilon_{r,2})}{2}\frac{K(\sqrt{1-k^2})}{K(k)} + \varepsilon_0\varepsilon_{r,1}\left(\frac{h}{s}\right) \tag{3}$$

Where ε_0 is the permittivity in free space, equal to 8.854 F/m, $\varepsilon_{r,1}$ is the relative permittivity of the material between parallel conductors, $\varepsilon_{r,2}$ is the relative permittivity of the substrate material, $\varepsilon_{r,3}$ is the relative permittivity of the material under test (MUT), $K(k)$ is the complete elliptic integral of the first kind, k is the ratio of the electrode gap (s) between the electrode width (w) and the electrode gap, given by $k = s/(s+w)$, and h is the electrode thickness. The structure of the interdigital electrode is considered to comprise multiple capacitances connected in parallel, resulting in a capacitive impedance. The capacitance or impedance value of the designed and fabricated electrodes can also be altered by the relative permittivity of the material under test ($\varepsilon_{r,3}$).

For measuring cannabinoids like CBD, the interdigital sensor operates using reflective coefficient (S_{11}) analysis. An RF signal excites the sensor, and the reflected signal is measured. When a CBD-containing sample is placed on the sensor, it alters the S_{11} value at specific resonance frequencies, allowing CBD concentration to be quantified. The electric field, generated between the interdigital electrodes, is crucial to S_{11}. This field interacts with the sample, and the sample's complex permittivity ($\varepsilon_r^* = \varepsilon_r' - j\,\varepsilon_r''$) affects wave reflection. ε_r' represents energy storage, while ε_r'' indicates energy loss. Changes in the solution's permittivity and loss factor influence the S_{11} value, enabling the sensor to detect variations in CBD concentration. The interdigital sensors are effective for measuring liquids in the microwave frequency range, with permittivity affecting capacitance, conductivity, and impedance. Higher CBD concentrations typically increase permittivity due to more polar molecules, altering the dielectric properties and the sensor's response. Variations in the concentration of CBD are expected to change the dielectric permittivity, a complex and frequency-dependent parameter, as described by (4).[41]

$$\varepsilon_r^*(f) = \varepsilon_r'(f) - \varepsilon_r''(f) \tag{4}$$

Where f is the frequency, the variation in frequency is expected to induce a change in the resonant frequency of the resonator, while the variation in dielectric losses in the MUT is related to the resonant frequency of the interdigital resonator, as described by (5).[42]

$$f_r = \frac{1}{2\pi\sqrt{LC}} \tag{5}$$

Where f_r is the resonant frequency, C is the capacitance of the interdigital resonator structure, and L is the parasitic inductance which can be estimated by (6).[42]

$$L \approx \frac{\mu_0 \times l \times \ln\left(\frac{2l}{w+s}\right)}{(N-1)} \tag{6}$$

Where N is the number of electrodes, l is the electrode length, s is the electrode gap, w is the electrode width (w) and μ_0 is the permeability of free Space ($4\pi \times 10^{-7}$ H/m).

For relatively small changes in dielectric permittivity, the capacitance (C) and the additional impedance (Z_L) of the loaded interdigital capacitive sensor change only slightly. This results in a minimal change in the reflection coefficient when using and measuring a single-port IDC sensor at microwave frequencies. Figure 2 (a) presents the equivalent circuit of a single-port network. The reflection coefficient[43] (Γ) is defined as $\Gamma = S_{11} = (Z_L - Z_0)/(Z_L + Z_0)$, where Z_0 is the port impedance, normalized to 50Ω. When Z_L approaches 50Ω, the reflection coefficient is small. The load impedance Z_L is mainly affected by the material under test which determines the reflection coefficient Γ. The MUT's microwave reflection spectra are acquired by sweeping the source's frequency and collecting S_{11} data. The resonance frequency, which is the frequency at which the magnitude of S_{11} is a minimum, is the most significant parameter of the microwave reflection spectrum. Therefore, this measurement focuses on observing the frequency shift (Δf) of the minimum reflection coefficient, which occurs at different materials under test as shown in Figure 2 (b).

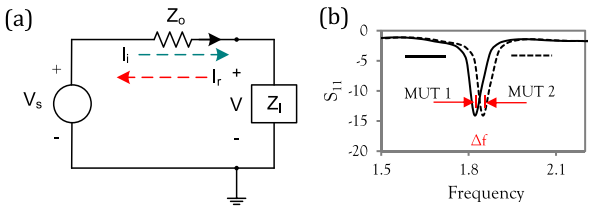

Figure 2. Equivalent circuit of a 1-port network and frequency shift on S_{11}. (a) Equivalent circuit of a 1-port network. (b) Frequency shift on S_{11}.

The relationship between the electric field and S_{11} is based on how the electric field generated by the interdigital sensor interacts with the solution's complex permittivity. The S_{11} value, which represents electromagnetic wave reflectivity, is affected by the sample's electrical properties. Changes in the electric field and permittivity impact S_{11}, enabling accurate CBD concentration measurement. By analyzing S_{11} when the sensor is excited with an RF signal, the presence of CBD can be quantified through shifts in S_{11} at specific resonance frequencies. This makes interdigital sensor-based S_{11} analysis an effective method for CBD measurement.

The fabricated interdigital electrode was characterized using a vector network analyzer (VNA) to measure the reflection coefficient (S_{11}) over a range of frequencies. It was tested with various CBD concentrations to establish a calibration curve relating the S_{11} response to CBD concentration. The electrode's performance was evaluated in terms of sensitivity, linearity, and repeatability.

https://doi.org/10.1021/acsomega.4c08811
ACS Omega 2024, 9, 51515−51524

B. Electrode Design and Simulations. The electrode designed for CBD concentration measurement features a simple interdigital structure to ensure accurate analysis. Modeling the electric field generated by this structure using finite element analysis (FEA) is essential for this study. Various software tools are available for analyzing interdigital electrode structures, materials, and designs using FEA. In this study, CST STUDIO SUITE is used to evaluate the electric field and single-port reflection characteristics (S_{11}). CST STUDIO SUITE is a specialized tool for 3D EM simulation of high-frequency components, commonly used for the fast and accurate analysis of high-frequency (HF) devices such as antennas, filters, couplers, and planar and multilayer structures. FEA is essential to obtain preliminary results and visualize the frequency response of the interdigital electrode before fabrication. CST STUDIO SUITE optimizes the shape and size of the interdigital electrode design. The designed electrode uses FR-4 printed material with the following surface characteristics: relative permittivity (εr) of 4.3, laminate thickness of 1.6 mm, loss tangent (tan δ) of 0.025, and metal layer thickness (t) of 0.035 mm. Simulations were performed for the electrode sizes used in the measurements. The sensing area is approximately 100 mm^2, consisting of 10 electrodes, with an equal number of signal and ground electrodes. The electrode width and gap between the electrodes are both 0.5 mm, and the electrode length is 10 mm, as shown in Figure 3(a). The selected electrode width and gap are appropriate for this work, including the design of the sensing area to fit the volume of the solution to be measured.

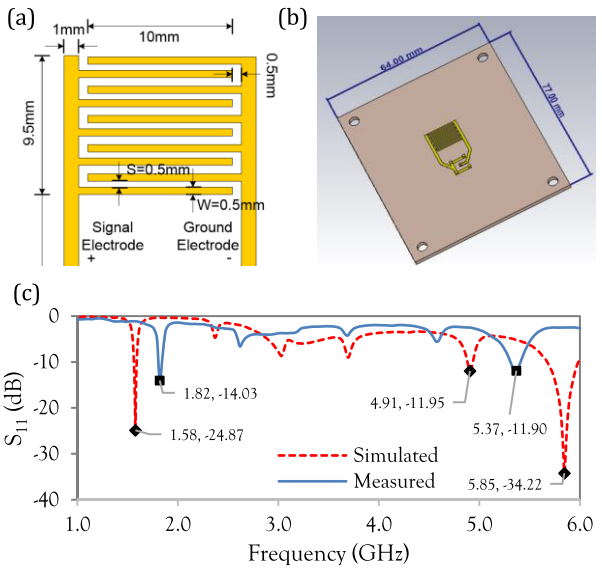

Figure 3. Interdigital electrode design and simulation. (a) Layout of the presented interdigital structure, (b) CST simulation model, and (c) S_{11} response between measured data and simulated data.

Figure 3(b) shows the 3D simulation model created in CST to optimize the dimensions of the designed interdigital electrode over a frequency range of 1.0−6.0 GHz. The simulation aimed to observe the response characteristics of the minimum reflection coefficient (S_{11}) and the electric field distribution before fabrication. The results indicated that the designed electrode achieves a minimum S_{11} at multiple frequencies, notably −24.87 dB at 1.58 GHz, − 11.95 dB at 4.91 GHz, and −34.22 dB at 5.85 GHz, as shown by the dashed lines in Figure 3(c).

The electrode's width and gap provided the lowest S_{11} curve with a sharp, narrow peak within the 1.6−1.8 GHz range considered in this study. The measured S_{11} spectrum, represented by a solid line, closely matched the simulated S_{11} spectrum in Figure 3(c), with only a minor difference of a few MHz between the two plots.

The solid lines represent the experimental results, which, although consistent with the simulation, show significant differences due to varying control parameters. Nevertheless, the simulation results provide a preliminary evaluation of the electrode properties before fabrication.

The simulation design involves evaluating the response of the interdigital electrode for noncontact measurement through a glass bottle container. An FR-4 substrate, measuring 20 mm × 20 mm × 1.6 mm, is placed on the electrode's sensing area. A 12 mm hole, matching the size of the glass bottle container, is drilled in the center to secure the glass bottle containing the sample solution. Additionally, a metal plane is included to confine the electric field within the sensor's sensing area, as shown in Figure 4(a). In this work, the electrodes were simulated and fabricated on (PCB) an FR-4 substrate of print circuit board with dimensions of 77 mm × 64 mm, with a high-frequency SMA connector.

The electric field distribution can be analyzed from the electric field lines using isolines obtained from the CST simulation. These isolines exhibit lower intensity in regions with high electric energy absorption, corresponding to the frequency where S_{11} shows the lowest reflection. To demonstrate the electric field potential of the designed electrode, it is essential to select a frequency where the S_{11} value is close to 0 dB. In this study, the frequency of 1.8 GHz is chosen for analysis. At this frequency, the electric field at −40 dB can penetrate up to 12 mm through the air, as shown in Figure 4 b). This suggests the electric field can also penetrate other test materials.

Due to the high cost of cannabidiol (CBD) extract used as a solvent, it is essential to minimize its usage in experiments. Additionally, because of the volatile nature of CBD, the development of noncontact measurement techniques is crucial for this work. In the next phase, the simulation involves examining the electric field distribution through a glass container (ε_r = 4.65, tan $\delta = 1 \times 10^{-12}$ S/m) with a diameter of 12 mm and a thickness of 0.4 mm.

The electric field distribution generated by a simulated electrode with a glass bottle container, as depicted in Figure 4 c), was compared to that of a simulated electrode without a glass bottle, as shown in Figure 4 b). The penetration depth of the electric field decreases due to the thickness of the glass bottle container and the change in permittivity. At an energy intensity of −40 dB, the electric field can penetrate approximately 6.5 mm into the glass bottle container. However, the simulation results indicate that the electric field can penetrate through the glass bottle container to the sample material inside. Therefore, noncontact measurement of the concentration of the sample solution is feasible.

Figure 5 illustrates the equivalent circuit of the interdigital electrode[44] proposed in this research. The circuit comprises electrical components that simulate the properties of the electrode structure in each layer, as follows:

https://doi.org/10.1021/acsomega.4c08811
ACS Omega 2024, 9, 51515−51524

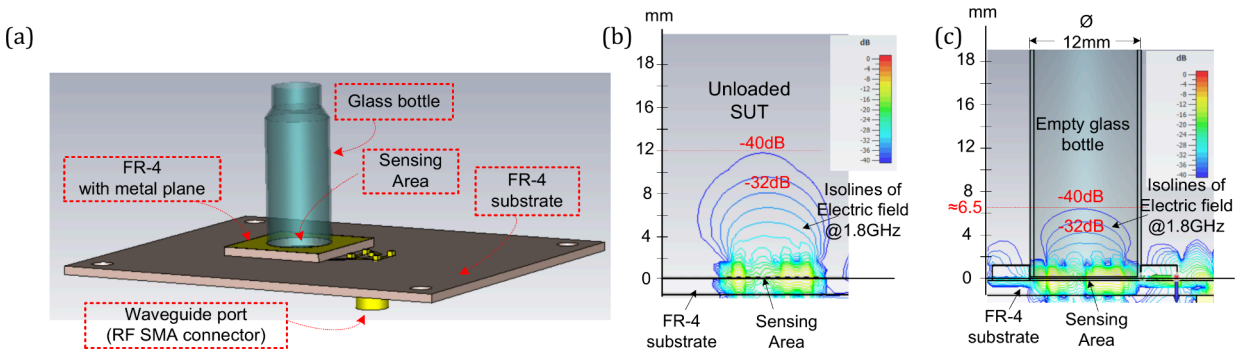

Figure 4. (a) Noncontact measurement simulation structure. Electric field distribution for noncontact measurement with (b) unloaded and (c) empty glass bottle.

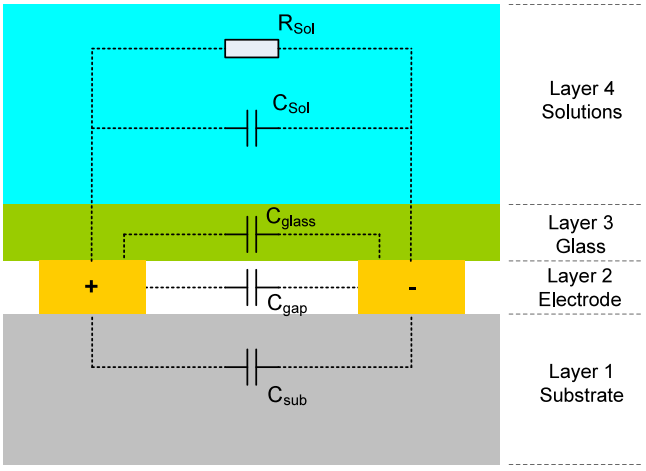

Figure 5. Equivalent circuit model for noncontact CBD measurements.

Layer 1: The substrate layer is modeled by a capacitor C_{sub}, representing the electrical capacitance of the base material.

Layer 2: The gap between electrodes is modeled by a capacitor representing the electrical capacitance of air.

Layer 3: The glass bottle container holding the CBD solution is modeled by a capacitor representing the electrical capacitance of glass.

Layer 4: The CBD solution is modeled by a parallel circuit of a resistor and a capacitor. The resistor represents the resistance of the solution, while the capacitor represents the electrical capacitance arising from charge mobility in the solution.

These four-layer components are modeled as a parallel circuit to reflect the physical characteristics of the electrode structure. This circuit modeling approach enables a more comprehensive and accurate analysis of the electrode's electrical characteristics.

C. Sample Preparation and Experiment Setup. For the measurement of CBD in real samples, such as cannabis extracts or infused products, appropriate sample preparation techniques are employed. This may involve extraction, dilution, or purification steps to ensure compatibility with the interdigital sensor. Methanol or acetonitrile is commonly used as the solvent for preparing standard solutions in the creation of a standard curve for HPLC analysis of CBD and THC. These solvents are highly compatible with both compounds and are well-suited for HPLC systems coupled with UV/vis detectors. In some cases, isopropanol or ethanol may also be used, but methanol and acetonitrile are the most common choices due to their high purity and stability.

Pure CBD is extracted from various parts of cannabis plants, such as marijuana and hemp. It is in powder form and packaged in a closed container. The pure CBD used in this work is (−)-Cannabidiol (CBD) (Mol. Formula $C_{21}H_{30}O_2$) with a purity of 99.02% (g/g), specified for laboratory use only. The CBD solution for the experiment was prepared by dissolving 10 mg of pure CBD in 10 mL of methanol, resulting in a CBD solution with a concentration of 1,000 ppm. This solution was further diluted with methanol to obtain various desired concentrations, as illustrated in Figure 6, and calculated

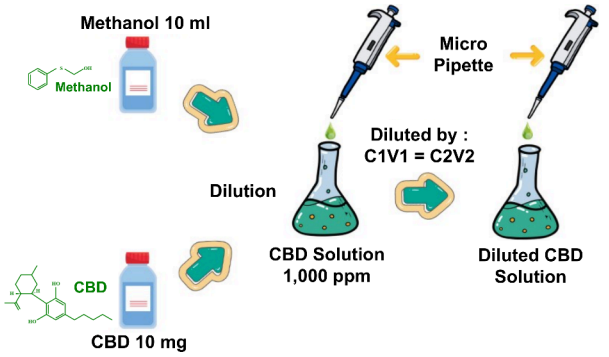

Figure 6. Preparation of CBD solution concentration.

based on the relationship between concentration and volume in (7). This work prepared CBD solutions with concentrations of 25 ppm, 125 ppm, 250 ppm, 500 ppm, and 1,000 ppm. The volumetric concentration ratios are shown in Table 1.

$$C_1V_1 = C_2V_2 \tag{7}$$

Where C_1 is the concentration of the stock solution, V_1 is the volume from the stock, C_2 is the final concentration of the

Table 1. Preparing the CBD Solution for the Experiment

C_2 (ppm)	V_2 (mL)	C_1 (ppm)	V_1 (mL)	methanol (mL)
25	2	1000	0.05	1.95
125	2	1000	0.25	1.75
250	2	1000	0.50	1.50
500	2	1000	1.00	1.00
750	2	1000	1.50	0.50
1000	2	1000	2.00	

https://doi.org/10.1021/acsomega.4c08811
ACS Omega 2024, 9, 51515−51524

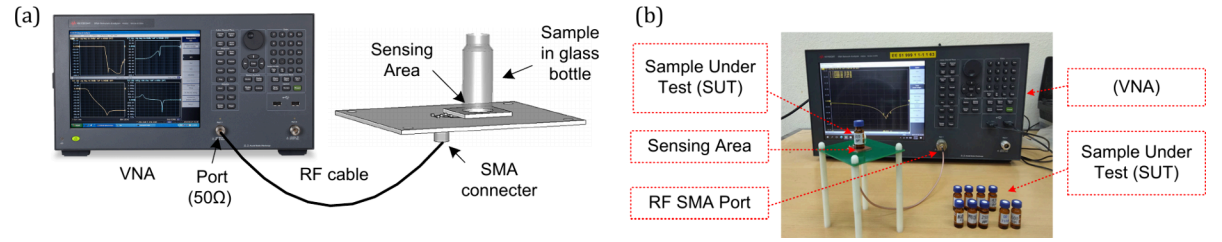

Figure 7. (a) Sketch of the measurement setup. (b) Experimental setup.

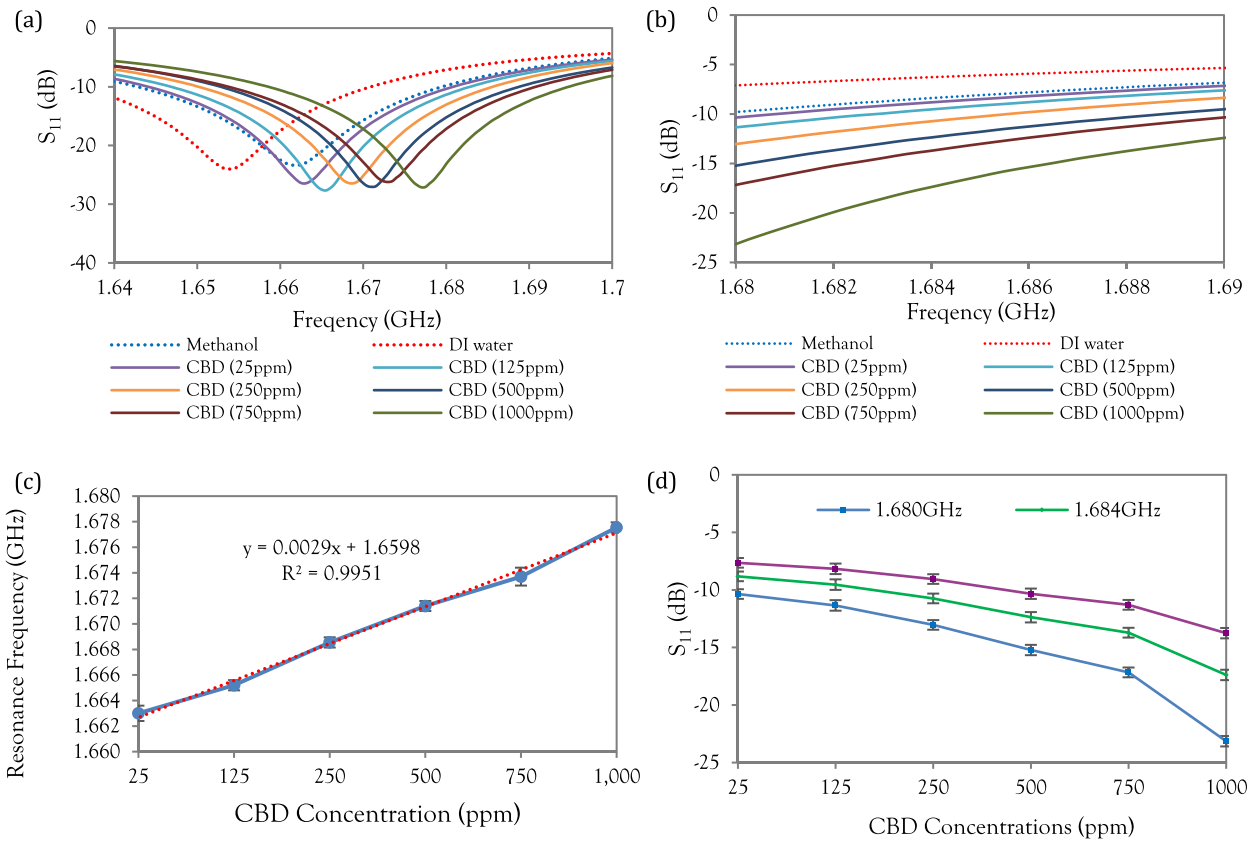

Figure 8. (a) Reflection coefficient spectra in the frequency range of 1.64 to 1.7 GHz with different CBD concentrations, (b) linear regression analysis of CBD concentrations with resonance frequencies, (c) 1.68−1.69 GHz frequency range of the reflection coefficient with various CBD concentrations, and (d) relation between S_{11} parameter magnitude and varying CBD concentrations, focusing on the frequency range of 1.68, 1.684, and 1.688 GHz.

diluted solution, and V_2 is the final volume of the diluted solution.

The prepared sample is placed on the sensor surface, and its reflection coefficient (S_{11}) is measured using a Vector Network Analyzer (VNA). The measured S_{11} values are compared for each CBD concentration to establish a calibration curve.

CBD measurement experiments were performed using an interdigital electrode at ambient temperature (25 °C). The experiments utilized 2 mL glass vials (HPLC vials) loaded on the electrode's sensing area and were conducted with an E5063A ENA Vector Network Analyzer (VNA). The sketch of the noncontact measurement setup for CBD solution concentration is shown in Figure 7 (a). Figure 7 (b) illustrates the experimental apparatus designed to evaluate the electrode's response to varying CBD concentrations. Glass vials, each containing 2 mL of CBD solution, were prepared across six concentration levels. To ensure data reliability, ten replicate measurements were conducted for each concentration. The electrode was securely mounted on a custom-designed rack, ensuring precise alignment with the vial contents.

A vector network analyzer (VNA) was employed to measure the electrode's frequency response between 1.64 to 1.7 GHz. with a 500 kHz sampling rate.

3. RESULTS AND DISCUSSION

The experimental results of various CBD concentrations corresponding to various S-parameters are shown in Figure 8 (a) the electrode output reflective signals are affected by CBD concentration. A minimum of −27.65 dB of S_{11}, measured around 1.66−1.68 GHz with CBD loaded, indicates that the impedance of the CBD-concentrated electrode matches that of 50 Ω. The resonance frequency of the S_{11} parameter shifted concerning the increasing CBD concentration, due to the change in the dielectric constant of the solution compared to the S_{11} parameter of pure methanol. Replication trials were conducted, and linear regression analyses were performed for

https://doi.org/10.1021/acsomega.4c08811
ACS Omega 2024, 9, 51515−51524

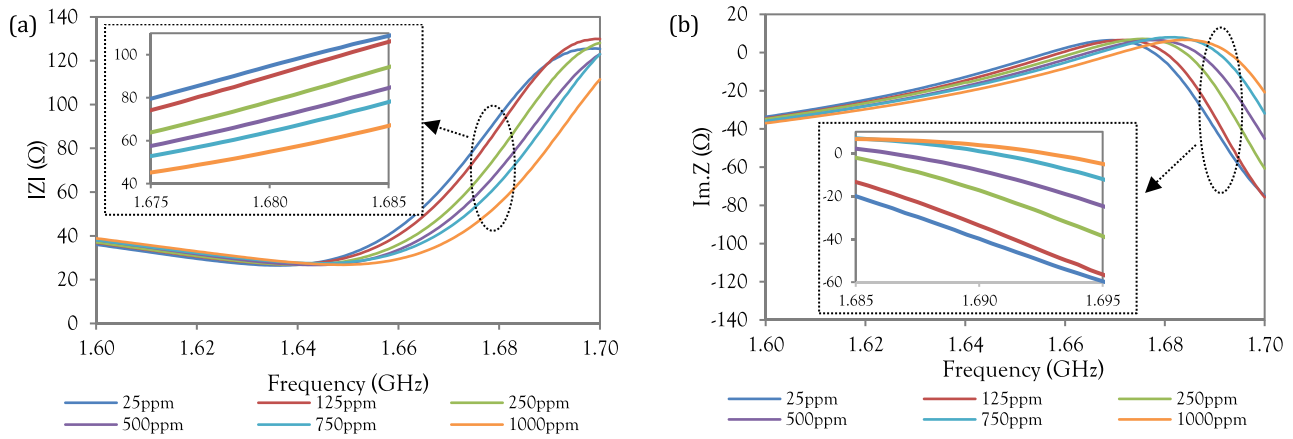

Figure 9. (a) CBD concentration corresponding to the amplitude of |Z|. (b) Imaginary part of the impedance of the electrode loaded at each CBD concentration in the frequency range of 1.6−1.7 GHz.

the tested data. The results of one experimental case are shown in Figure 8 (a). As shown in Figure 8 (b), a good linear relationship exists between the concentration of CBD and the resonance frequency of the reflection coefficient. This indicates that the designed electrode can be used to measure CBD levels. Furthermore, a strong linear correlation (R^2 = 0.9951) between the CBD concentration and resonance frequency was observed, suggesting that our method can accurately determine CBD concentration. Based on these results, there is a linear variation in the sensor's resonant frequency, with a shift of Δf = 2.9 MHz in the frequency range of interest. This corresponds to a high sensitivity of about 145 MHz per 50 ppm. Our method is also capable of measuring the minimum CBD concentration of 25 ppm.

To visualize the distribution of data from the replication experiments, the results are presented as an error bar in Figure 8 (c). A statistically significant difference was observed among the median values of each CBD concentration. From Figure 8 (b), the resonance frequencies of replication tests at concentrations of 25, 125, 250, 500, and 1000 ppm are 1.663 ± 0.0006 GHz, 1.6652 ± 0.0004 GHz, 1.669 ± 0.0004 GHz, 1.671 ± 0.0004 GHz, 1.673 ± 0.0007 GHz, and 1.678 ± 0.0004 GHz, respectively. It was seen that the uncertainty errors of resonance frequency for all CBD concentration levels are around 0.02%−0.038% reading, or equivalently, less than 700 Hz. Experimental results showed that the error or variance in resonance frequency caused by changes in CBD concentration did not overlap when the CBD concentration differed by 50 ppm. Therefore, this method can be used to clearly distinguish and quantify CBD concentrations that differ by 50 ppm. These resonance frequency measurements of S_{11} are more stable and accurate and thus less prone to errors and false readings.

The S_{11} reflective coefficient related to the sweep high frequency according to Figure 12 in the 1.68−1.69 GHz frequency range, further magnified in Figure 8 (c), revealed that each CBD concentration corresponded to the amplitude of the reflection coefficient. The amplitude of S_{11} gradually decreased when the CBD concentrations increased. However, the variation in the amplitude of S_{11} for different CBD concentrations is different, which can be used to distinguish the CBD concentration level. Three specific frequency ranges were selected for study: 1.68, 1.684, and 1.688 GHz. The relationship between the amplitude of S_{11} and various CBD concentrations at these frequencies was examined and is presented in Figure 8 (d).

Figure 8 (d) shows the variation of the amplitude of S_{11} for the replication test versus the CBD concentrations at each sensing frequency from 1.680 to 1.688 GHz. As the CBD concentrations increased, the values of S_{11} decreased significantly within 125 ppm and more rapidly declined after 750 ppm. The different slopes of these curves can be used to distinguish the CBD concentration level. The inset in Figure 8 (d) shows that there was a linear relationship between the concentrations of CBD and the S_{11} amplitude when the concentrations range were 25−125 ppm, 125−250 ppm, 250−500 ppm, 500−750 ppm, and 750−1000 ppm. For all the replication CBD concentration tests, it can be seen that the sensitivity of S_{11} amplitude versus the various CBD concentrations at 1.68 GHz is higher than that at 1.684 and 1.688 GHz. The different slopes of the curves can be used to distinguish the five ranges of the CBD concentrations. They can also represent the sensitivities of this method which were about 1 dB/100 ppm, 1.7 dB/125 ppm, 2.2 dB/250 ppm, 1.9 dB/250 ppm, and 6 dB/250 ppm for the CBD concentration, respectively. It suggests that the S_{11} amplitude measurement is quite good for detecting the CBD concentration with high concentration at frequencies slightly above the resonance frequency. The shift of the amplitude of S_{11} is used to analyze the measured limit. The variation of S_{11} can be distinguished when the concentration is stepped from 25 to 125 ppm in increments of 10 ppm. The S_{11} amplitude for the 50 ppm sample is approximately 10.8 dB, which is slightly higher than that of the uncertainty error of an average S_{11} amplitude measurement used in this work. Thus, the measured limit of the sensor can be as low as 50 ppm in terms of the variation of the amplitude of S_{11}.

This measuring resolution of CBD concentration determined by the measurement of S_{11} parameter amplitude is consistent with the one obtained from the resonant frequency measurements of the reflection coefficient as previously described. In this study, it was found that the S_{11} magnitude measurement results at low CBD concentrations have a higher variance than in the case of high concentrations. This may be attributed to the variable energy loss in the electric field caused by the unsteady movement of free ions in CBD solution.

As seen in Figure 9 (a), the impedance of the electrode loaded with varying CBD concentrations approaches 50 Ω

https://doi.org/10.1021/acsomega.4c08811
ACS Omega 2024, 9, 51515−51524

within the frequency range of 1.66−1.68 GHz, aligning with the previously stated matching range. Especially, in the frequency range of 1.675−1.685 GHz, the change of impedance concerning CBD concentration is also at a noticeable level to distinguish the CBD concentration. The greatest impedance change can be observed at 1.68 GHz. For impedance at 1.68 GHz, changes for varying CBD concentrations fall within a range of 55−95 Ω, with higher CBD concentrations corresponding to lower impedance values due to the conductivity of the solution. The impedance values within this range are potentially suitable for designing a measurement circuit; however, such a circuit would likely require exceptionally high precision to effectively differentiate between concentrations.

Figure 9 (b) illustrates the frequency response of the imaginary part of the electrode's impedance (Im.Z) for various CBD concentrations within the frequency range of 1.6−1.7 GHz. The negative values indicate the capacitive properties of the electrode, resulting from the dielectric characteristics of the methanol solution mixed with cannabis extract.

In the frequency range of 1.6−1.66 GHz, the imaginary part of the impedance cannot distinguish between different CBD concentrations and converges to zero due to resonance. It then returns to negative values at approximately 1.68 GHz. However, in the frequency range of 1.685−1.695 GHz, the imaginary part of the impedance can differentiate CBD concentrations, with higher CBD concentrations yielding lower absolute values of the imaginary impedance. It reveals that the changes in the imaginary part of the impedance between CBD concentrations in the ranges of 125−250 ppm, 250−500 ppm, and 500−750 ppm differ significantly, in descending order of value. Consequently, measuring the imaginary part of the impedance to differentiate CBD concentrations is highly accurate within the 125−750 ppm range, while measurements in the 25−125 ppm and 750−1000 ppm ranges may be subject to greater error. The methanol-CBD solutions of 5 replication tests at each concentration measured by the proposed resonance frequency measurement were confidently validated against those prepared by dissolving pure CBD in methanol, as shown in Figure 10. It was observed that the R-squared correlation coefficient was approximately 0.9986, indicating a strong correlation, and the accurate error was 0.17% of the reading.

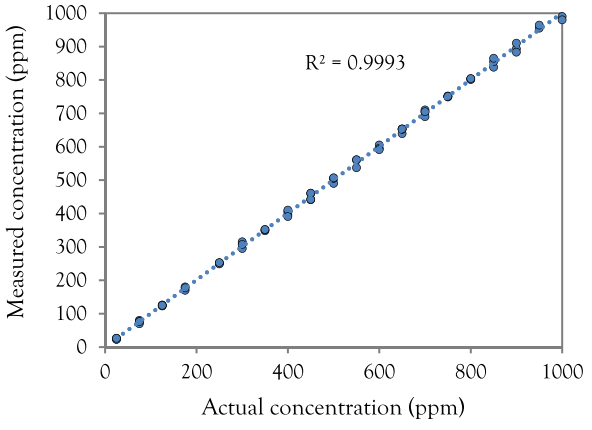

Figure 10. Correlation between the measured value and the actual value.

4. CONCLUSIONS

This paper demonstrates the feasibility of using interdigital electrodes for noncontact CBD concentration measurement through analysis of the reflection coefficient (S_{11}). The electrodes were designed and optimized using CST STUDIO SUITE software, with simulations conducted to evaluate the electric field penetration and interaction with CBD solutions inside glass containers. The simulation results confirmed that the electric field intensity could effectively penetrate the container to interact with the CBD solution, supporting the feasibility of the proposed sensing method.

Experimental measurements of the S_{11} frequency response in the 1.64−1.7 GHz range further validated this method. The results showed a significant correlation between CBD concentration and resonance frequency, with shifts in resonance frequency reflecting changes in impedance matching, energy absorption, and dielectric properties of the solution. The experimental results significantly demonstrated a high degree of precision in the resonance frequency measurements of the S_{11} parameter correlated with CBD concentration levels. The uncertainty was found to be less than 0.038% of the reading, or equivalently, less than 700 Hz for all CBD concentration levels. This resonance frequency measurement demonstrates the potential to differentiate CBD concentrations with a resolution of up to 50 ppm, which is a significant value for practical applications. With this level of precision, the design of a variable high-frequency oscillator or frequency sweep generator for this detection system becomes highly feasible in practice, both in terms of ease of development and convenience of use. Furthermore, this resolution facilitates the future development of highly efficient portable detection devices. In addition to resonance frequency analysis, the relationship between the magnitude of S_{11} and CBD concentration was investigated.

The results indicated that the S_{11} magnitude decreased while the resonance frequency increased in inverse proportion to the rise in CBD content. Low-concentration range sensitivity (e.g., 1 dB per 100 ppm below 125 ppm) provides the potential of precise circuit design. However, achieving ultrahigh precision will require careful calibration and advanced circuit designs. Impedance frequency response analysis at 1.8 GHz further corroborated these findings. The impedance values demonstrated an inverse correlation with CBD concentration, indicative of increased electrical conductivity at higher concentrations. While sensitivity in the range of tens of ohms per 250 ppm was noted, it presents challenges for designing highly sensitive detection circuits. The capacitive properties of the CBD solutions, reflected in the imaginary part of the impedance, were also analyzed, showing potential for distinguishing concentrations in wide ranges (e.g., 125−750 ppm). The study shows the potential of interdigital electrodes for nondestructive CBD concentration measurement, with significant implications for quality control in CBD oil production. This preliminary study, conducted under controlled laboratory conditions using CBD-methanol solutions, serves as a foundational step in developing innovative contactless detection methods.

Future work will focus on expanding the applicability of this method to more complex matrices, such as cannabis and hemp derivatives, which often contain additional compounds. To address the challenges caused by such complex media, future studies will explore the use of advanced signal conditioning

https://doi.org/10.1021/acsomega.4c08811
ACS Omega 2024, 9, 51515−51524

circuits and enhanced data processing techniques, including deep learning and generative AI algorithms, to improve measurement accuracy and selectivity. Additionally, the method's potential for biological matrices including blood and urine will be investigated, where interference from other molecular species presents significant challenges. Collaborations with specialized laboratories will ensure that these studies are conducted under controlled conditions, adhering to ethical and legal standards.

AUTHOR INFORMATION

Corresponding Author

Kanadit Chetpattananondh − *Department of Electrical and Biomedical Engineering, Faculty of Engineering, Prince of Songkla University, Hat Yai 90110, Thailand*; orcid.org/0000-0003-2847-1667; Phone: +66 74 287045; Email: kanadit.c@psu.ac.th; Fax: +66 74 459395

Authors

Kanitsorn Boonrat − *Department of Electrical and Biomedical Engineering, Faculty of Engineering, Prince of Songkla University, Hat Yai 90110, Thailand*

Pinyada Jaroenkunpanit − *Department of Chemical Engineering, Faculty of Engineering, Prince of Songkla University, Hat Yai 90110, Thailand*

Phairote Wounchoum − *Department of Electrical and Biomedical Engineering, Faculty of Engineering, Prince of Songkla University, Hat Yai 90110, Thailand*

Vasan Jantarachote − *Department of Electrical and Biomedical Engineering, Faculty of Engineering, Prince of Songkla University, Hat Yai 90110, Thailand*

Pakamas Chetpattananondh − *Department of Chemical Engineering, Faculty of Engineering, Prince of Songkla University, Hat Yai 90110, Thailand*

Complete contact information is available at: https://pubs.acs.org/10.1021/acsomega.4c08811

Author Contributions

K.B. performed original draft, writing, software, validation, and data curation. P.J. performed validation, resource gathering, visualization, and data curation. P.W. performed methodology, conceptualization, software, formal analysis, validation, data curation, and investigation. V.J. performed methodology, conceptualization, software, formal analysis, validation, data curation, and investigation. P.C. performed conceptualization, investigation, writing−review and editing, visualization, and supervision. K.C. performed conceptualization, methodology, investigation, writing−original draft, writing−review and editing, formal analysis, visualization, supervision, project administration, and funding acquisition.

Notes

The authors declare no competing financial interest.

ACKNOWLEDGMENTS

This research was financially supported by the National Science, Research, and Innovation Fund (NSRF) and Prince of Songkla University (grant no. ENG6701110b). The Department of Electrical Engineering and the Department of Chemical Engineering, the Faculty of Engineering, Prince of Songkla University, the Faculty of Engineering and Technology, Rajamangala University of Technology Srivijaya, Trang campus, and the Ministry of Science and Technology (Thailand) are acknowledged for other support. The authors also would like to thank the anonymous reviewers for their valuable comments.

REFERENCES

(1) Mechoulam, R.; Hanuš, L. O.; Pertwee, R.; Howlett, A. C. Early Phytocannabinoid Chemistry to Endocannabinoids and Beyond. *Nat. Rev. Neurosci.* **2014**, *15* (11), 757−764.

(2) Velasco, G.; Sánchez, C.; Guzmán, M. Towards the Use of Cannabinoids as Antitumor Agents. *Nat. Rev. Cancer.* **2012**, *12* (6), 436−444.

(3) Moltke, J.; Hindocha, C. Reasons for Cannabidiol Use: A Cross-Sectional Study of CBD Users, Focusing on Self-Perceived Stress, Anxiety, and Sleep Problems. *J. Cannabis Res.* **2021**, *3* (1), 5.

(4) McRae, G.; Melanson, J. E. Quantitative Determination and Validation of 17 Cannabinoids in Cannabis and Hemp Using Liquid Chromatography-Tandem Mass Spectrometry. *Anal. Bioanal. Chem.* **2020**, *412*, 7381−7393.

(5) Nemeškalová, A.; Hájková, K.; Mikulů, L.; Sýkora, D.; Kuchař, M. Combination of UV and MS/MS Detection for the LC Analysis of Cannabidiol-Rich Products. *Talanta* **2020**, *219*, No. 121250.

(6) Shokoohi Rad, S.; Dalali, N.; Baheri, T. Combination of Magnetic Solid-Phase Extraction with Dispersive Liquid-Liquid Microextraction Followed by GC-MS for Trace Analysis of Synthetic Cannabinoids in Plasma Samples. *Micro Nano Lett.* **2020**, *15*, 545−549.

(7) Citti, C.; et al. A Novel HPLC-MS/MS Method for the Simultaneous Quantification of CBD, THC and Their Acid Precursors in Olive Oil Extracts. *J. Pharm. Biomed. Anal.* **2018**, *150*, 596−602.

(8) Jiang, X.; et al. Voltammetric Determination of Cannabidiol in Hemp Seed Oil Using a Boron-Doped Diamond. *Electrode Anal. Lett.* **2020**, *53* (15), 2517−2531.

(9) Smith, E.; et al. Surface-Enhanced Raman Spectroscopy for the Detection and Quantification of Cannabinoids. *Anal. Chim. Acta* **2021**, *1161*, 338472.

(10) Deconinck, E.; et al. Detection and Quantification of Synthetic Cannabinoids in Herbal Matrices and CBD Oils Using ATR-FTIR Spectroscopy and Chemometrics. *Talanta* **2019**, *195*, 516−524.

(11) Yüksel, S.; Schwenke, A. M.; Soliveri, G.; Ardizzone, S.; Weber, K.; Cialla-May, D.; Hoeppener, S.; Schubert, U. S.; Popp, J. Trace Detection of Tetrahydrocannabinol (THC) with a SERS-Based Capillary Platform Prepared by the In Situ Microwave Synthesis of AgNPs. *Anal. Chim. Acta* **2016**, *939*, 93−100.

(12) Milliken, S.; Fraser, J.; Poirier, S.; Hulse, J.; Tay, L. L. Self-Assembled Vertically Aligned Au Nanorod Arrays for Surface-Enhanced Raman Scattering (SERS) Detection of Cannabinol. *Spectrochim. Acta, Part A* **2018**, *196*, 222−228.

(13) Plouffe, B. D.; Murthy, S. K. Fluorescence-Based Lateral Flow Assays for Rapid Oral Fluid Roadside Detection of Cannabis Use. *Electrophoresis.* **2017**, *38* (3−4), 501−506.

(14) Stevenson, H.; Bacon, A.; Joseph, K. M.; Gwandaru, W. R. W.; Bhide, A.; Sankhala, D.; Dhamu, V. N.; Prasad, S. A Rapid Response Electrochemical Biosensor for Detecting THC in Saliva. *Sci. Rep.* **2019**, *9* (1), 12701.

(15) Li, Y.; Uddayasankar, U.; He, B.; Wang, P.; Qin, L. Fast, Sensitive, and Quantitative Point-of-Care Platform for the Assessment of Drugs of Abuse in Urine, Serum, and Whole Blood. *Anal. Chem.* **2017**, *89* (16), 8273−8281.

(16) Lee, J. R.; Choi, J.; Shultz, T. O.; Wang, S. X. Small Molecule Detection in Saliva Facilitates Portable Tests of Marijuana Abuse. *Anal. Chem.* **2016**, *88* (15), 7457−7461.

(17) Pholsiri, T.; Lomae, A.; Pungjunun, K.; Vimolmangkang, S.; Siangproh, W.; Chailapakul, O. A Chromatographic Paper-Based Electrochemical Device to Determine Δ^9-Tetrahydrocannabinol and Cannabidiol in Cannabis Oil. *Sens. Actuators B* **2022**, *355*, No. 131353.

(18) Boertien, M.; Smith, R.; Stewart, B.; Mazyan, W.; Bressan, N.; Ahmadi, A. Development of a Low-Cost Portable Sensor for Detection of Tetrahydrocannabinol (THC) in Saliva. In *CMBES Proceedings*; **2018**, *41*.
(19) Gaggiotti, S.; Palmieri, F.; Della Pelle, F.; Sergi, M.; Cichelli, A.; Mascini, M.; Compagnone, D. Piezoelectric Peptide-hpDNA Based Electronic Nose for the Detection of Terpenes; Evaluation of the Aroma Profile in Different Cannabis Sativa L.(Hemp) Samples. *Sens. Actuators B* **2020**, *308*, No. 127697.
(20) Mehrabi, P.; Hui, J.; Janfaza, S.; O'Brien, A.; Tasnim, N.; Najjaran, H.; Hoorfar, M. Fabrication of SnO2 Composite Nanofiber-Based Gas Sensor Using the Electrospinning Method for Tetrahydrocannabinol (THC) Detection. *Micromachines* **2020**, *11* (2), 190.
(21) Mamishev, A. V.; Sundara-Rajan, K.; Yang, F.; Du, Y.; Zahn, M. Interdigital Sensors and Transducers. *Proc. IEEE* **2004**, *92* (5), 808−845.
(22) Afsarimanesh, N.; Nag, A.; Alahi, M. E. E.; Han, T.; Mukhopadhyay, S. C. Interdigital Sensors: Biomedical, Environmental and Industrial Applications. *Sens. Actuators, A* **2020**, *305*, No. 111923.
(23) Chetpattananondh, K.; Tapoanoi, T.; Phukpattaranont, P.; Jindapetch, N. A Self-Calibration Water Level Measurement Using an Interdigital Capacitive Sensor. *Sens. Actuators A* **2014**, *209*, 175−182.
(24) Ahmad, S.; Khalid, N.; Mirzavand, R. Detection of Soil Moisture, Humidity, and Liquid Level Using CPW-Based Interdigital Capacitive Sensor. *IEEE Sens. J.* **2022**, *22* (11), 10338−10345.
(25) Chetpattananondh, P.; Thongpull, K.; Chetpattananon-dh, K. Interdigital Capacitance Sensing of Moisture Content in Rubber Wood. *Computers Electronics Agric.* **2017**, *142*, 545−551.
(26) Akhter, F.; Alahi, M. E. E.; Siddiquei, H. R.; Gooneratne, C. P.; Mukhopadhyay, S. C. Graphene Oxide (GO) Coated Impedimetric Gas Sensor for Selective Detection of Carbon Dioxide (CO2) with Temperature and Humidity Compensation. *IEEE Sens. J.* **2021**, *21* (4), 4241−4249.
(27) Hammarling, K.; Engholm, M.; Andersson, H.; Sandberg, M.; Nilsson, H.-E. Broad-Range Hydrogel-Based pH Sensor with Capacitive Readout Manufactured on a Flexible Substrate. *Chemosensors.* **2018**, *6* (3), 30.
(28) Al Imran, M. N.; Glass, S. W.; Fifield, L. S.; Ali, M. Flexible Fabric-Based IDC Sensors for Conformal Curved Surface Applications. *IEEE Sens. J.* **2021**, *21* (1), 812−820.
(29) Chen, X.; et al. Integrated Interdigital Electrode and Thermal Resistance Micro-Sensors for Electric Vehicle Battery Coolant Conductivity High-Precision Measurement. *J. Energy Storage.* **2023**, *58*, No. 106402.
(30) Afsarimanesh, N.; Mukhopadhyay, S. C.; Kruger, M. Performance Assessment of Interdigital Sensor for Varied Coating Thicknesses to Detect CTX-I. *IEEE Sens. J.* **2018**, *18* (10), 3924−3931.
(31) Ullah, A.; Zulfiqar, M. H.; Khan, M. A.; Zubair, M.; Mehmood, M. Q.; Massoud, Y. Fast Response Facile Fabricated IDE-Based Ultra-Sensitive Humidity Sensor for Medical Applications. *ACS Omega.* **2023**, *8* (19), 16842−16850.
(32) Yunos, M. F. A. M.; Manczak, R.; Guines, C.; Mansor, A. F. M.; Mak, W. C.; Khan, S.; Ramli, N. A.; Pothier, A.; Nordin, A. N. RF Remote Blood Glucose Sensor and a Microfluidic Vascular Phantom for Sensor Validation. *Biosensors* **2021**, *11* (12), 494.
(33) Rahman, M. S. B. A.; Mukhopadhyay, S. C.; Yu, P. L. Novel Sensors for Food Inspections. *Sens. Transducers* **2010**, *114* (3), 1.
(34) Rossignol, J.; Harrabi, A.; Stuerga, D.; Pribetich, P.; Bailly, G.; Leblois, T. Critical Influence of Dielectric Sensitive Material and Manufactured Process in Microwave Gas-Sensing: Application of Ammonia Detection with an Interdigital Sensor. *ACS Omega.* **2020**, *5* (20), 11507−11514.
(35) Sappati, K. K.; Bhadra, S. Printed Acoustic Sensor for Low Concentration Volatile Organic Compound Monitoring. *IEEE Sens. J.* **2021**, *21* (8), 9808−9818.
(36) Xie, L.; Zia, A. I.; Mukhopadhyay, S.; Burkitt, L. Electrochemical Impedimetric Sensing of Nitrate Contamination in Water. In *2015 9th International Conference on Sensing Technology (ICST)*, Auckland, New Zealand, December 2015; IEEE: Piscataway, NJ, 2015; pp 257−262.
(37) Yin, J.; Zhang, J.; Feng, L.; Guan, Y.; Gao, W.; Jin, Q. Free Chlorine Ultra-Sensitive Detection in Tap Water via an Enrichment-Sensing Process by an Interdigitated Microelectrode Sensor. *Electrochim. Acta* **2022**, *419*, No. 140428.
(38) Niu, G.; Wang, Z.; Xue, Y.; Yan, J.; Dutta, A.; Chen, X.; Wang, Y.; Liu, C.; Du, S.; Guo, L.; Zhou, P.; Cheng, H.; Yang, L. Pencil-on-Paper Humidity Sensor Treated with NaCl Solution for Health Monitoring and Skin Characterization. *Nano Lett.* **2023**, *23* (4), 1252−1260.
(39) Kythe, P. K. *Handbook of Conformal Mappings and Applications*; CRC Press: Boca Raton, FL, 2019.
(40) Bhuiyan, R. H.; Dougal, R. A.; Ali, M. Proximity Coupled Interdigitated Sensors to Detect Insulation Damage in Power System Cables. *IEEE Sensors J.* **2007**, *7* (12), 1589−1596.
(41) Gregory, A. P.; Clarke, R. N. *Tables of the Complex Permittivity of Dielectric Reference Liquids at Frequencies up to 5 GHz*; NPL Report **2012**, EDM 33.
(42) Li, L.; Xu, F.; Wu, K.; Delprat, S.; Chakef, M. Slow-Wave Line Filter Design Using Full-Wave Circuit Model of Inter-Digital Capacitor. In *2005 European Microwave Conference*, Paris, France, October 2005; IEEE: Piscataway, NJ, 2005; Vol. *1*, pp 4-pp.
(43) Pozar, D. M. *Microwave Engineering*; John Wiley & Sons: 2011.
(44) Korek, E. M.; Teotia, R.; Herbig, D.; Brederlow, R. Electrochemical Impedance Spectroscopy for Ion Sensors with Interdigitated Electrodes: Capacitance Calculations, Equivalent Circuit Models and Design Optimizations. *Biosensors.* **2024**, *14* (5), 241.

https://doi.org/10.1021/acsomega.4c08811
ACS Omega 2024, 9, 51515−51524